

PM Design of IPMSM using Parameterized Finite Element Model

Huijuan Liu, Haijiao Zhang, Jingxiong Zhang

School of Electrical Engineering, Beijing Jiaotong University, Beijing, 100044, China

*Corresponding author, e-mail: hjliu@bjtu.edu.cn

Abstract

In this paper, a parameterized transient finite element model for permanent magnet (PM) dimension analysis and performance simulation of a V-shape interior permanent magnet synchronous motor (IPMSM) with 8 poles is developed. The relationships between induced electromotive force (EMF) and PM dimension, cogging torque and PM dimension are analyzed; the geometries of PM structure are optimized by performing response surface methodology (RSM); a new type of flux-barrier is designed to weaken the flux leakage, and the performances of the sample IPMSM are simulated.

Keywords: interior permanent magnet synchronous motor (IPMSM), parameterized finite-element analysis, induced EMF, response surface methodology (RSM), flux-barrier

Copyright © 2013 Universitas Ahmad Dahlan. All rights reserved.

1. Introduction

The Interior permanent magnet synchronous motor (IPMSM) are widely used in home application, industrial, and electric and hybrid vehicle propulsion. Due to their superior performance characteristics that include high efficiency, high torque density, a wide constant power operating range, compact structure, and fast dynamic response, the IPMSM is an excellent candidate for vehicle propulsion [1-10]. A large number of IPMSM applications require minimized torque ripple for reduced vibration and acoustic noise, and smooth operation of the motor. In addition, low torque pulsations in motor drives are essential for high-performance speed and position control applications.

In IPMSMs, the permanent magnets (PMs) are deposited inside the rotor core, which is not only for avoiding the separation of PM caused by the centrifugal force at high speed, but also for employing a hybrid torque generation that includes electromagnetic torque, reluctance torque and cogging torque [2]. The electromagnetic torque is produced by the interaction of the rotor PMs' field and stator currents; the reluctance torque is generated from the special rotor structure, i.e. the rotor saliency; and the cogging torque is caused by the interaction between PMs and slotted iron structure.

Figure 1 illustrates a V-shape PM rotor structure of an IPMSM, where a PM isThis variation of the PM structure around the rotor will bring about significant saliency effect, which can produce reluctance torque in addition to the electromagnetic torque [3]. By utilizing unique hybrid torque generation, high-efficiency performance can be achieved.

According to the analysis of hybrid torque characteristics from before, the increase of reluctance torque production due to higher rotor saliency can compensate the decrease of magnet torque production when generating electromagnetic torque production. In general, the higher rotor saliency results in less electromagnetic torque. As a result, the currents fed to the stator windings can be reduced, and the copper loss caused in armature windings decreases correspondingly, which is helpful to improve motor efficiency performance.

The output torque quality can be improved by reducing the torque ripple, which is related to the harmonics in the induced EMF of stator windings. Reducing the cogging torque will also improve the output torque quality. Methods for reducing cogging torque and for minimizing the induced EMF harmonic contents to minimize the torque ripple appear in [4, 5].

In order to achieve high performance of IPMSM sensorless driving system, some researchers have addressed the torque ripple problem in IPMSMs from the control side [6, 7], while others worked from a motor design point of view for optimal rotor shape design [8, 9].

The PM size affects not only the quality of the induced EMF but also the cogging torque [10, 11]. Some researches for the PM size design limited to build their model with only one parameter of the PM size changed.

In this paper, a detailed analysis of the relationship between induced EMF variations with different PM size is presented by using the parameterized transient finite element analysis model of an 8-pole number of V-shape IPMSM. The induced EMF of stator winding and the cogging torque is calculated using the parameterized transient simulation model when one or two of the parameters is changed.

In addition, owing to the PM is located inside the rotor; the magnetic field is directly short-circuited through the rotor iron core. Thus the magnetic flux leakage is formed [12]. In order to reduce the rotor magnetic flux leakage, the flux-barrier (or magnetic bridge) is introduced to isolate the magnetic field between the magnetic poles [13]. Traditional flux-barrier of IPMSM is a rectangular shape; in this paper, the shape of flux-barrier is redesigned to improve the magnetic isolation effect and the motor performance by using 2-D finite element analysis (FEA) [14].

2. Optimal Design of PM Structure in IPMSM

The analysis IPMSM model is built from a sample traction motor used in an electrical vehicle propulsion system, as shown in Figure 1. It has 8 poles and 48 slots with distributed windings placed in the stator part. In the rotor core, the single-layer, V-shape PM segments are inserted into the radial cavity at each pole region. Because the structure of the motor is symmetrical and to save simulation time, only 1/4 model of this motor is presented (Figure 1). As shown in Figure 1, the dimension parameters of the PM is consists of three components, i.e., the angle (α), width (w) and thickness (t); and in this sample motor, the α , w and t are 90 degree-160 degree, 14.5mm-18mm, and 3.5mm-5.5mm respectively. The main dimensions of this sample machine are listed in Table 1.

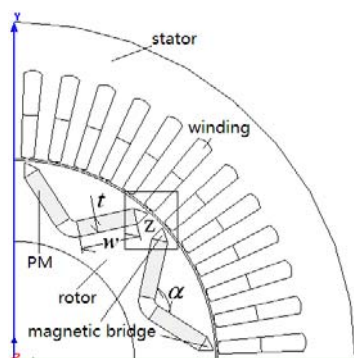


Figure 1. Model of V-shape IPMSM

Table 1. Main Dimensions of the IPMSM

Stator OD (mm)	210	Rated Speed (rpm)	720
Rotor OD (mm)	124	Pole number	8-pole
Stator ID (mm)	125.2	Stator Slots	48
Rotor ID (mm)	74	Stack Length (mm)	70

Table 2. Variable Range

Variable parameters	α (degree)	w (mm)
Range	90 ~160	14.5~18
Step size	5	0.25

2.1. Research of PM Structure

In IPMSMs, the magnet shape and its magnetization direction determine the distribution of the no-load air-gap magnetic field. The industry practice is to start with a given magnet shape and then obtain the magnetic flux characteristics by 2-D or 3-D FEA calculations. The phase induced EMF waveforms obtained from these characteristics are compared to some standard waveforms, and the FEA is repeated until satisfactory results are obtained [15].

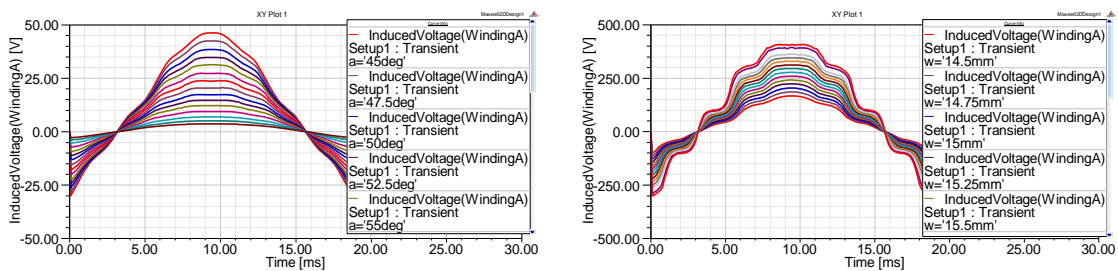
Owing to thickness t of the PM structure has no influence on the induced EMF [16], and then only two PM dimension α and w are considered to affect the induced EMF. In this paper, a parameterized transient finite element analysis model of the sample V-shape IPMSM is built to compute the induced EMF waveforms when α and w are changing respectively. The detail variation range and step size of α and w are listed in Table 2.

The induced EMF computation by parameterized finite element analysis is directly based on the magnetic flux density and field intensity on each element. The results are

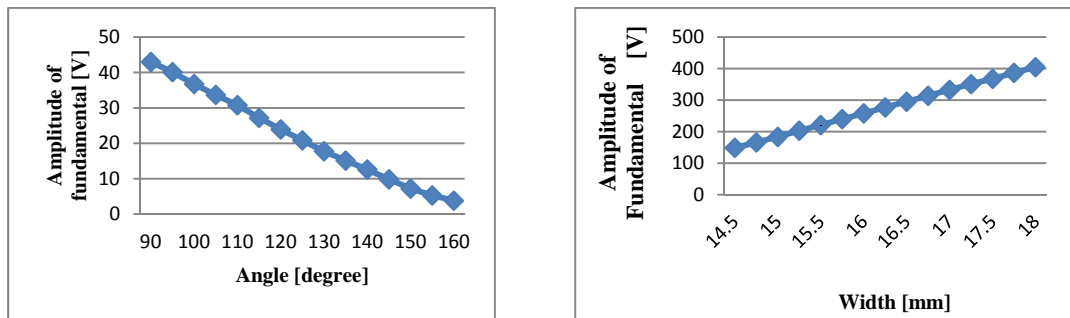
considered accurate because the complicated geometry of the IPMSM and nonlinearity of the materials are taken into full account. The induced EMF voltages are computed for α and w changing respectively. And all the induced EMF versus parameters α or w are shown in Figure 2(a) and (b) respectively.

By using MATLAB software, when α or w is changing, the harmonic analysis (FFT) of the induced EMF is performed, the THDs and the fundamental amplitudes of induced EMF are acquired, and the curve of fundamental amplitude versus α or w are shown in Figure 3 and Figure 4 respectively.

From Figure 3(a), we can find that the larger the angle α is, the smaller the amplitude of EMF is; and Figure 3(b) shows that the larger the width w is, the larger the fundamental magnitude of EMF is. Figure 4 shows that the THD of induced EMF decreases with the increase of w , and first increase then decrease with the increase of α , and the turning point of the THD- α curve is 115degree, i.e. when $\alpha=115$ degree, the THD of induced EMF is the minimum of 14.7%.



(a) Induced EMF when α is changing (b) Induced EMF when w is changing
Figure 2. Induced EMF versus Parameters α and w



(a) Fundamental amplitude when α is changing (b) Fundamental amplitude when w is changing
Figure 3 Fundamental Amplitude of EMF

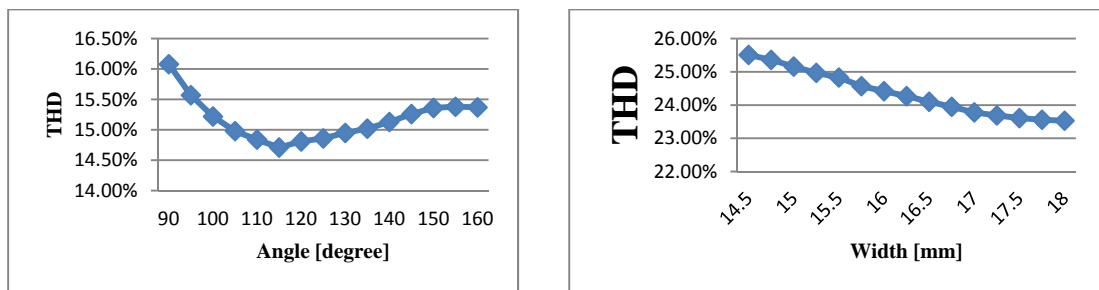


Figure 4(a). THD of induced EMF when α is changing

Figure 4(b). THD of induced EMF when w is changing

2.2. Response Surface Methodology (RSM)

Response surface methodology (RSM) is an interpolation technique that fits a multidimensional function to its function values at some sample points on an arbitrary function domain [17, 18]. A brief introduction of RSM is given below. Let $R^+ = \{x \in R, x \geq 0\}$ be the set of non-negative real numbers and suppose a scalar function $H : R^+ \rightarrow R$ be continuous with $H(0) \geq 0$. A radial basis function on R^d is defined in the form:

$$H(\|X\|) \quad (1)$$

Where $X \in R^d$, $\|\cdot\|$ is the Euclidean norm.

In general, the reconstruction of an objective or constraint function $f(X) : R^d \rightarrow R$ on the basis of its value f_i at a given set of sample points $X_i \in R^d (i = 1, 2, \dots, N)$ under some radial basis functions $\{H_j\}_{j=1}^N$ is:

$$f(x) = \sum_{j=1}^N c_j H_j = \sum_{j=1}^N c_j H(\|X - X_j\|). \quad (2)$$

The coefficients $C = \{c_j\}_{j=1}^N$ are determined by the following linear algebraic equation:

$$C = H^{-1}F \quad (3)$$

Where $H_{ij} = H(\|X_i - X_j\|)$ is the interpolation matrix and $F = \{f_j\}_{j=1}^N$.

In the PM optimal design process, the parameterized finite element analysis model of the IPMSM is built to investigate the influence on fundamental magnitude and THD of induced EMF when the PM size α and w are changing at the same time, and thickness $t=4.5\text{mm}$. For all the parameters in the sweeping analysis, uniform steps are used to solve for the optimal design such that 5 degree and 0.25mm for parameters α and w , so there are totally $15 \times 15 = 225$ times FEM computations. In our FEA parameter sweeping computation, it takes around 5.0 hours to obtain all the solutions.

Since the magnetic flux is essentially independent of the PM thickness t , all the fundamental magnitudes of EMF versus α and w are given in Figure 5, and all the THD's of induced EMF versus the sample parameters α and w are given in Figure 6. From Figure 5, it can be seen that the fundamental magnitude is decreasing when α increases while w decreases. Figure 6 shows that the minimum THD value appears at the linear equation of $w = -0.25\alpha + 40$, and the minimum THD is about 22%.

The cogging torque is inherent torque of an IPMSM, and it is also influenced by PM size. In finite element analysis, by removing all windings, setting all conductivities to zero, the cogging torque of an IPMSM can be computed and we have found that the thickness t of the PM has no influence of the cogging torque. The cogging torque curves while parameters α or w is changing are given in Figure 7(a) and (b) respectively. After post processing from Figure 7(a) and (b), we can get the curves of the cogging torque magnitude versus parameters α and w as shown in Figure 8(a) and (b) respectively. From Figure 8(a), it can be seen that, as the α increasing, the cogging torque first increases then decreases with it, and the turning point of the cogging torque is 100degree. Figure 8(b) shows that as the w is increasing, the cogging torque is becoming larger.

When α and w are changing at the same time, the cogging torque versus α and w is shown in Figure 9, and it shows that the minimum cogging torque appears at the linear equation $w = -0.4\alpha + 56$. Therefore, the optimal PM size of the sample motor is determined: angle $\alpha = 105\text{degree}$, width $w = 14.5\text{mm}$ and thickness $t = 4.5\text{mm}$.

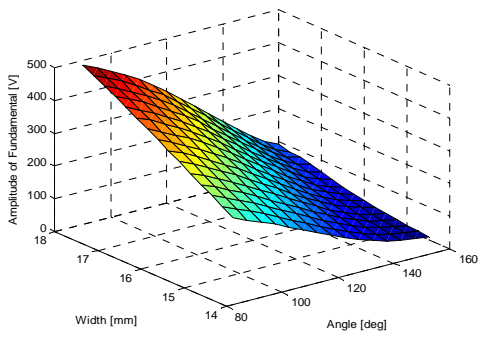


Figure 5. Fundamental Amplitude when α and w both Change

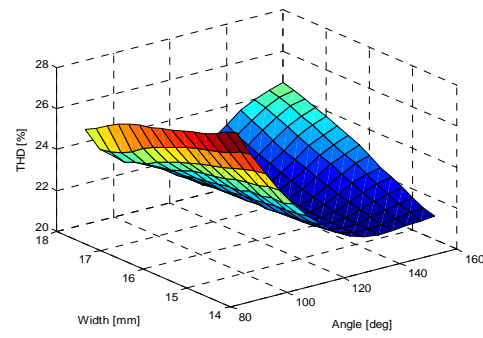
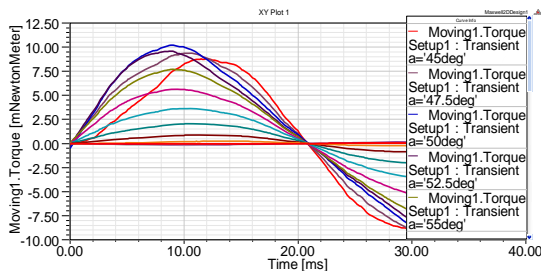
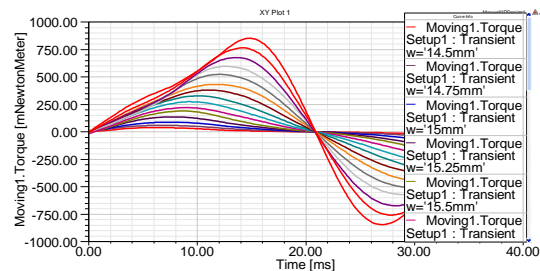


Figure 6. THD of Induced EMF when α and w both Change

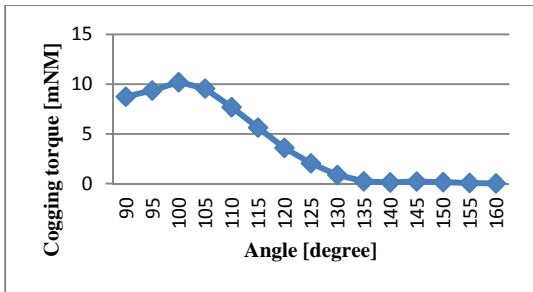


(a) Cogging torque waveforms when α is changing

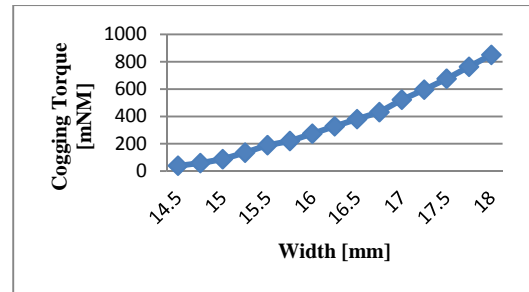


(b) Cogging torque waveforms when w is changing

Figure.7 Cogging Torque versus Time



(a) The magnitude of cogging torque versus α



(b) The magnitude of cogging torque versus w

Figure 8. The Magnitude of Cogging Torque versus α and w

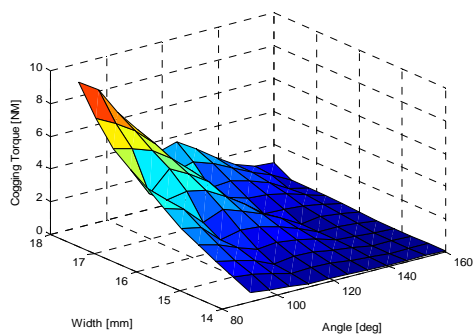


Figure 9. Cogging Torque versus α and w

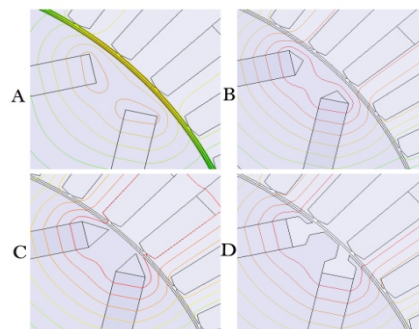


Figure 10. Flux Distribution with Different Shape of Magnetic Bridge

2.3. Re-design of Flux-Barrier Structure in IPMSM

The IPMSM rotor inner geometry design is very complicated owing to many design factors, as well as the mechanical robustness between each part must be fully considered. Therefore, the mentioned flux-barrier designs in IPMSM rotor are optimized efficiently with the help of finite element analysis method. There are many advantages of IPMSM rotor configuration. However, due to the PM is located inside the rotor; some magnetic field can be directly short-circuited in the rotor between the PM poles. The flux is essentially leakage flux; it does not cross the air gap and does not contribute to torque production. The design of flux-barrier is a solution for solving this issue [19]. In this paper, there are four representative flux-barrier designs are built in IPMSM models for reducing the flux leakage. The part Z in Figure 1 was zooming in as Figure 10 with four types of flux-barrier, i.e. no flux-barrier; small triangle flux-barrier; large triangle flux-barrier and the polygonal flux-barrier connected to the air gap. In order to compare the difference of flux leakage of the four types of flux-barrier, according to [20, 21], the leakage coefficient σ is defined as: $\sigma_A = A_{z1}/A_{z2}$. Where A_{z1} denotes the total flux Φ_m of the PM supply; A_{z2} denotes the total mutual flux of stator windings. By using the finite element analysis, the leakage coefficient σ of the four types of flux-barrier can be calculated: $\sigma_A=1.32$; $\sigma_B=1.26$; $\sigma_C=1.14$; $\sigma_D=1.09$. We can find that the leakage coefficient σ_D is the smallest, and the polygonal magnetic bridge connected to the air gap as shown in Figure 10 is the best shape among the four types of magnetic bridge. So the polygonal magnetic bridge is introduced in the sample motor.

3. Performance Simulation of the Sample IPMSM

3.1. No-load Characteristics

The finite element analysis is used to calculate the performances of the sample IPMSM. The cross section and mesh division of the sample motor are shown in Figure 11(a) and (b) respectively.

When the IPMSM operates at no-load mode, there is only the PM fields in the motor, the three-phase stator windings on open circuit and the rotor is rotating at a constant speed, then the EMF will be induced in the armature windings. By using FEM, we have also investigated the air-gap flux density distribution and the induced back EMF of the stator winding. Figure 12 shows the air-gap flux density of the IPMSM at no-load operation, and the waveform of the flux density is closed to sine wave. The results show that the magnetic field in the air gap is reasonable. Figure 13 shows the calculated harmonic contents of the air-gap flux density waveform, and Figure 14 shows the cogging torque curve versus rotor position and its magnitude is about 1.2Nm.

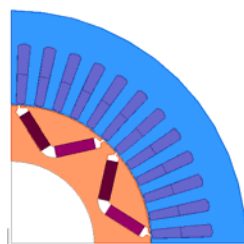


Figure 11(a). The cross section of the IPMSM

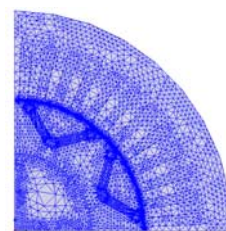


Figure 11(b). The mesh division of the IPMSM

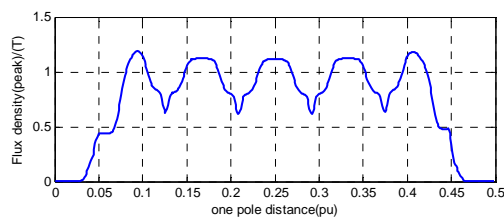


Figure 12. Air-gap Flux Density at No-load Operation

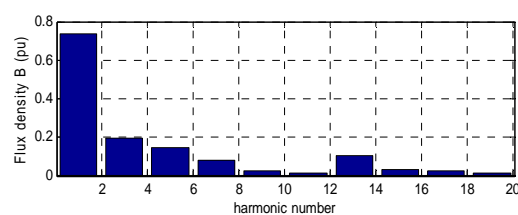


Figure 13. Harmonic Contents of the Air-gap Flux Density

3.2. Calculation of the L_q and L_d

The calculation is conducted with the rotor rotating at 742rpm, not the rated synchronous speed 750rpm, and the slip is about 0.01. The PMs in rotor are deleted and has no rotor magnetic field, while the three-phase stator windings are fed with AC current at 50Hz, the current peak is 1A. Figure 15 shows the flux linkage of the stator phase A. The results show that the maximum flux linkage of phase A is 0.0328Wb, the minimum flux linkage is 0.025Wb. By using flux linkage results, the L_q , L_d , X_d and X_q can be calculated. $L_d=0.0328/1=0.0328H$, $X_d=\omega L_d=20.6\Omega$; $L_q=0.025/1=0.025H$, $X_q=\omega L_q=15.7\Omega$.

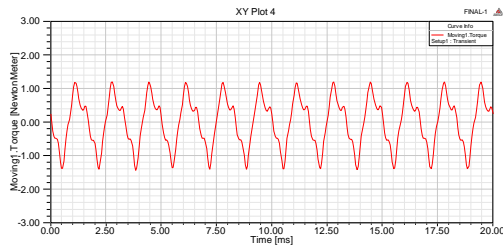


Figure 14. The Cogging Torque Curve versus Rotor Position

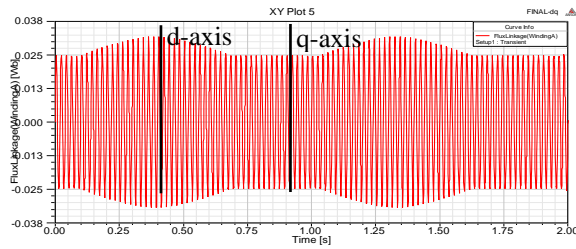
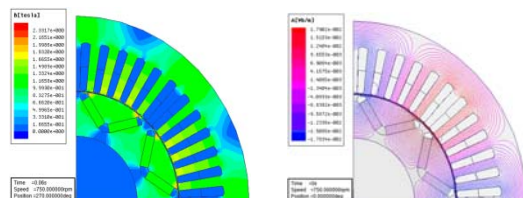


Figure 15. Flux Linkage of Phase A

3.3. Loaded Operation Performances

The magnetic flux distribution of the sample IPMSM at full load operation can be investigated when the rated three-phase sine AC voltages 150V (peak, 50Hz) are imposed to the stator windings. At this rated operation mode, the flux density of the cross-section of the sample IPMSM is shown in Figure 16(a), and the part saturation phenomenon is clear; the flux distribution over the cross-section is shown in Figure 16(b). From Figure 16(a), we can find that the average flux density and the maximum flux density in rotor core are about 1.4T and 1.9T respectively, the maximum flux density in stator are occurred at stator tooth, about 1.9T, the average flux density in stator yoke is about 0.8T to 1.4T. The induced EMF of the sample motor is shown in Figure 17.



(a) Flux density (b) Flux distribution
Figure 16. The Magnetic Fields Features of the IPMSM in Loaded Operation

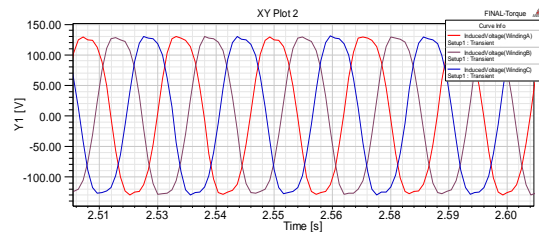


Figure 17. Induced EMF of the Stator Windings

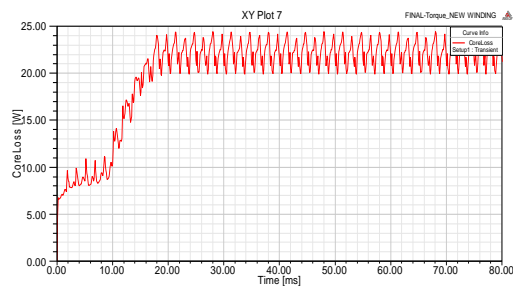


Figure 18. Core Losses at Full Load Operation

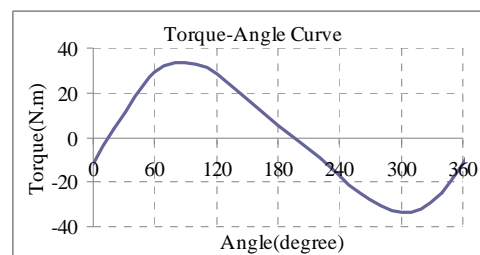


Figure 19. Torque Characteristics of the IPMSM

The transient core loss at the full-load operation is simulated with dynamic core loss model and the core loss curves are shown in Figure 18. The core loss is about 22W, which are mainly induced in the stator core and rotor core. If the initial phase angle of the three phase voltages is changed from 0 to 360 degree at step with 10 degree, during the every simulation, the peak of the voltage is 150V. The sinusoidal torque curve shown in Figure 19 also named as the power-angle characteristic of the synchronous machine, and the rated power angle of the sample IPMSM is 60 degree.

4. Conclusion

This paper focuses on the analysis of the relationship between the performances and PM size using the parameterized transient finite element analysis model of an 8-pole, V-shape IPMSM. The induced EMF of stator winding and the cogging torque is calculated by using parameterized transient FEA model when one or two of the PM parameters is changed. Response surface methodology (RSM) is used to optimize the PM size parameters: angle α , width w , and thickness t . The minimum THD value appears at the linear equation of $w=0.25\alpha+40$, and the minimum cogging torque appears at the linear equation $w=-0.4\alpha+56$. The optimal PM parameters are: angle $\alpha=105$ degree, width $w=14.5$ mm and thickness $t=4.5$ mm. Then, the redesign of the flux-barrier is developed to reduce the flux leakage of the rotor. Finally, the performances of the sample motor are computed using 2-D FEA model. The magnetic fields distribution, the torque characteristics, the core losses, the q -axis inductance L_q and the d -axis inductance L_d of the prototype machine are presented. All studies show that the V-shape IPMSMs are potential to apply in hybrid vehicles and electric vehicles driving system.

Acknowledgement

This work was supported by NJTU Paper Foundation of China and The Jing Yuan Education Fund of Beijing Jiaotong University.

References

- [1] Jang-Young Choi, Yu-Seop Park, Seok-Myeong Jang. Experimental Verification and Electromagnetic Analysis for Performance of Interior PM Motor According to Slot/Pole Number Combination. *IEEE Transactions on Magnetics*. 2012; 48(2):987-990.
- [2] GH Kang, JP Hong, GT Kim. Analysis of cogging torque in interior permanent magnet motor by analytical method. *KIEE Int. Trans. Electr. Mach. Energy Conver. Syst.* 2006; 11B(2):1-8.
- [3] R Islam, I Husain, A Fardoun, K McLaughlin. Permanent magnet synchronous motor magnet designs with skewing for torque ripple and cogging torque reduction. *IEEE Trans. Ind. Appl.* 2009; 45(1): 152-161.
- [4] N Bianchi, S Bolognani. Design techniques for reducing the cogging torque in surface-mounted PM motors. *IEEE Trans. Ind. Appl.* 2002; 38(5): 1259–1265.
- [5] SM Hwang, JB Eom, YH Jung. Various design techniques to reduce cogging torque by controlling energy variation in permanent magnet motors. *IEEE Trans. Magn.* 2001; 37(4): 2806-2809.
- [6] M Dai, A Keyhani, T Sebastian. Torque ripple analysis of a PM brushless DC motor using finite element method. *IEEE Trans. Energy Convers.* 2004; 19(1): 40–45.
- [7] V Petrovic, R Ortega, AM Stankovic, G Tadmor. Design and implementation of an adaptive controller for torque ripple minimization in PM synchronous motors. *IEEE Trans. Power Electron.* 2000; 15(5): 871–880.
- [8] Jeonghu Kwack, Seungjae Min, Jung-Pyo Hong. Optimal Stator Design of Interior Permanent Magnet Motor to Reduce Torque Ripple Using the Level Set Method. *IEEE Transactions on Magnetics*. 2010; 46(6): 2108-2111.
- [9] Y Li, J Zou, Y Lu. Optimum design of magnet shape in permanent magnet synchronous motors. *IEEE Trans. Magn.* 2003; 39(6): 3523-3526.
- [10] Aimeng Wang, Yihua Jia, Shuhui Dong. *Design and Analysis of a Novel Interior Permanent Magnet Machine for Hybrid Electric Vehicle Traction*. International Conference on Electrical Machines and systems (ICEMS). Beijing. 2011: 1-4.
- [11] Chaohui Zhao, Ning Yang, Xinwei Wang. *The Structure Optimization of IPM Synchronous Machine*. IEEE International Symposium on Industrial Electronics. Vigo. 2007: 1092-1096.

-
- [12] Xianming Deng, Kang Wang, Shengzhu Xia, Ningning Li, Kun Hu. *Design and Finite Element Analysis of Permanent Magnet Synchronous Motor with Novel Magnetic Bridge*. International Conference on Computing Control and Industrial Engineering (CCIE). Wuhan. 2010: 97-100.
- [13] Ron D Bremner. *Bridge Stresses and Design in IPM Machines*. Proceedins of IEEE Eurocon 2009. Petersburg. 2009: 655-662.
- [14] MH Nagrial, J Rizk, A Hellany. *Design and Performance of Interior Permanent Magnet Motors with Saturating Magnetic Bridge*. IEEE International Conference on Electric Machines and Drives. Antalya. 2009: 922-927.
- [15] ZQ Zhu, D Howe. Influence of Design Parameters on Cogging Torque in Permanent Magnet Machines. *IEEE Trans. Energy Conversion*. 2000; 15(4): 407-412.
- [16] DA Staton, TJE Miller, SE Wood. *Maximising the saliency ratio of the synchronous reluctance motor*. Proc. Inst. Elect. Eng.-Electr. Power Appl., Brighton. 1993; 140(4):249–259.
- [17] SL Ho, YS Yang, GZ Ni, HC Wong. A response surface methodology based on improved compactly supported radial basis function and its application to rapid optimizations of electromagnetic devices. *IEEE Trans. Magn*. 2005; 41(6): 2111-2117.
- [18] Yingchao Zhang, Huijuan Liu. Performance Analysis of Doubly Excited Brushless Generator with Outer Rotor for Wind Power Application. *TELKOMNIKA Indonesia Journal of Electrical Engineering*. 2012; 10(3): 471-476.
- [19] Ding Shuye, Zhang Ning. Analysis of Electromagnetic Properties of Doubly-fed Turbine Generator. *TELKOMNIKA Indonesia Journal of Electrical Engineering*. 2013; 11(2): 783-788.
- [20] TJE Miller. *Brushless Permanent-Magnet and Reluctance Motor Drives*. Oxford: Clarendon Press. 1989: 448-455.
- [21] Liu Jianzhong. An Approach to Get No-Load Leakage Flux Coefficient of PM Machine by Maxwell 2D. *Explosion-proof Electric Machine*. 2010; 45(5): 24-26. (in Chinese).